

# Resonant Scattering of Surface Plasmon Polaritons by Dressed Quantum Dots

Danhong Huang<sup>1</sup>, Michelle Easter<sup>2</sup>, Godfrey Gumbs<sup>3</sup>,  
A. A. Maradudin<sup>4</sup>, Shawn-Yu Lin<sup>5</sup>, Dave Cardimona<sup>1</sup>,  
and Xiang Zhang<sup>6</sup>

<sup>1</sup>*Air Force Research Laboratory, Space Vehicles Directorate,  
Kirtland Air Force Base, NM 87117, USA*

<sup>2</sup>*Department of Mechanical Engineering, Stevens Institute of Technology,  
1 Castle Point Terrace, Hoboken, NJ 07030, USA*

<sup>3</sup>*Department of Physics and Astronomy,  
Hunter College of the City University of New York,  
695 Park Avenue New York, NY 10065, USA*

<sup>4</sup>*Department of Physics and Astronomy and Institute for Surface and Interface Science,  
University of California, Irvine, CA 92697, USA*

<sup>5</sup>*Department of Physics, Applied Physics, and Astronomy,  
Department of Electrical, Computer,  
and Systems Engineering, and Future Chips Constellation,  
Rensselaer Polytechnic Institute, 110 8th Street, Troy, New York 12180, USA*

<sup>6</sup>*National Science Foundation Nanoscale Science and Engineering Center,  
3112 Etcheverry Hall, University of California at Berkeley, Berkeley, CA 94720*

(Dated: September 29, 2018)

## Abstract

The resonant scattering of surface plasmon-polariton waves by embedded semiconductor quantum dots above the dielectric/metal interface is explored in the strong-coupling regime. In contrast to non-resonant scattering by a localized dielectric surface defect, a strong resonant peak in the scattering field spectrum is predicted and accompanied by two side valleys. The peak height depends nonlinearly on the amplitude of surface plasmon-polariton waves, reflecting the feedback dynamics from a photon-dressed electron-hole plasma inside the quantum dots. This unique behavior in the scattering field peak strength is correlated with the occurrence of a resonant dip in the absorption spectrum of surface plasmon-polariton waves due to interband photon-dressing effect. Our result on the scattering of surface plasmon-polariton waves may be experimentally observable and applied spatially selective illumination and imaging of individual molecules.

Most of the previously reported research carried out on the optical properties of condensed matter, including well-known optical absorption and inelastic light scattering, made use of a weak probe field as a perturbation to the system under investigation [1]. In this weak-coupling limit, the optical response of electrons depends only on the material characteristics. However, with increased field intensity, the optical properties of materials are found to depend nonlinearly on the strength of the external perturbation [2].

Strong photon-electron interaction in semiconductors is known to produce dressed states [3–5] with a Rabi gap for electrons and create substantial nonlinearity in the semiconductor [6–8]. The presence of an induced polarization field, treated as a source term [9] arising from photo-excited electrons in metals, allows for a *resonant* scattering of surface plasmon-polariton waves [10]. This is quite different from the *non-resonant* scattering of surface plasmon-polariton waves by a localized dielectric surface defect [11, 12] or by surface roughness [13].

In this Letter, based on the obtained analytical solution [14, 15] for the Green’s function of the coupled quantum dot and semi-infinite metallic material system, we report for the first time our semi-analytic solutions of the self-consistent equations for strongly coupled electromagnetic field dynamics and quantum kinetics of electrons in a quantum dot above the surface of a thick metallic film. In our formalism, strong light-electron interaction is manifested in the photon-dressed electronic states and in the feedback from induced optical polarization of dressed electrons to the incident light as well. Our calculated results predict a strong resonant peak in the scattering field spectrum, which is accompanied by two side valleys at the same time. Furthermore, we have discovered that the peak height varies nonlinearly with the amplitude of the surface plasmon-polariton waves. This clearly demonstrates the effect due to feedback dynamics from photon-dressed electron-hole (e-h) plasma inside quantum dots. In addition, this unique observation in the scattering field spectrum is proven to be correlated with a resonant dip observed in the absorption spectrum [10] of surface plasmon-polariton waves which can be directly attributed to an effect of the inter-band photon-dressing of electronic states.

Our model system consists of a semi-infinite metallic material and a semiconductor quantum dot above its surface. A surface plasmon-polariton (SPP) wave is locally excited through a surface grating by a normally-incident light. This propagating SPP wave further excites

an inter-band e-h plasma within the quantum dot. The induced local optical polarization field of the photo-excited e-h plasma is resonantly coupled to the SPP wave to produce a splitting in degenerate e-h plasma and SPP modes with an anti-crossing gap.

By using the Green's function  $\mathcal{G}_{\mu\nu}(\mathbf{r}, \mathbf{r}'; \omega)$ , we may express Maxwell's equation for the electric field component  $\mathbf{E}(\mathbf{r}; \omega)$  of an electromagnetic field in a semi-infinite non-magnetic medium in position-frequency space as a three-dimensional integral equation, i.e.,

$$E_\mu(\mathbf{r}; \omega) = E_\mu^{(0)}(\mathbf{r}; \omega) - \frac{\omega^2}{\epsilon_0 c^2} \sum_\nu \int d^3\mathbf{r}' \mathcal{G}_{\mu\nu}(\mathbf{r}, \mathbf{r}'; \omega) \mathcal{P}_\nu^{\text{loc}}(\mathbf{r}'; \omega), \quad (1)$$

where  $\mathbf{E}^{(0)}(\mathbf{r}; \omega)$  is a solution in the absence of semiconductor quantum dots,  $\mathbf{r} = (x_1, x_2, x_3)$  is a three-dimensional position vector,  $\omega$  is the angular frequency of the incident light,  $\epsilon_0$  and  $c$  are the permittivity and speed of light in vacuum,  $\mathcal{P}^{\text{loc}}(\mathbf{r}; \omega)$  is an off-surface local polarization field that is generated by optical transitions of electrons in a quantum dot, which generally depends on the electric field in a nonlinear way and should be determined by the optical Bloch equations. Additionally, the position-dependent dielectric constant  $\epsilon_b(x_3; \omega)$  is equal to  $\epsilon_d$  for the semi-infinite dielectric material in the region  $x_3 > 0$ , but is given by  $\epsilon_M(\omega)$  for the semi-infinite metallic material in the region  $x_3 < 0$ .

By assuming a surface plasmon-polariton wave propagating within the  $x_1 - x_2$ -plane, we can write

$$\mathbf{E}^{(0)}(\mathbf{r}; \omega_{\text{sp}}) = E_{\text{sp}} e^{i\mathbf{k}_0(\omega_{\text{sp}}) \cdot \mathbf{D}_0} \frac{c}{\omega_{\text{sp}}} \left[ i\hat{\mathbf{k}}_0 \beta_3(k_0, \omega_{\text{sp}}) - \hat{\mathbf{x}}_3 k_0(\omega_{\text{sp}}) \right] e^{i\mathbf{k}_0(\omega_{\text{sp}}) \cdot \mathbf{x}_{\parallel}} e^{-\beta_3(k_0, \omega_{\text{sp}}) x_3}, \quad (2)$$

where  $\mathbf{x}_{\parallel} = \{x_1, x_2\}$ ,  $\hat{\mathbf{k}}_0$  and  $\hat{\mathbf{x}}_3$  are the unit vectors in the  $\mathbf{k}_0 = k_0(\omega_{\text{sp}}) \{\cos \theta_0, \sin \theta_0\}$  and  $x_3$  directions,  $E_{\text{sp}}$  is the field amplitude,  $\omega_{\text{sp}}$  is the field frequency,  $\theta_0$  is the angle of the incident surface plasmon-polariton wave with respect to the  $x_1$  direction,  $\mathbf{D}_0 = \{-x_{1g}, -x_{2g}\}$  is the position vector of the center of a surface grating, and the two wave numbers in Eq. (2) are given by

$$k_0(\omega_{\text{sp}}) = \frac{\omega_{\text{sp}}}{c} \sqrt{\frac{\epsilon_d \epsilon_M(\omega_{\text{sp}})}{\epsilon_d + \epsilon_M(\omega_{\text{sp}})}}, \quad (3)$$

and

$$\beta_3(k_0, \omega_{\text{sp}}) = \sqrt{k_0^2(\omega_{\text{sp}}) - \frac{\omega_{\text{sp}}^2}{c^2}} \quad (4)$$

with  $\text{Re}[k_0(\omega_{\text{sp}})] \geq 0$  and  $\text{Re}[\beta_3(k_0, \omega_{\text{sp}})] \geq 0$ . Here, the in-plane wave vector  $k_0$  is produced by the surface-grating diffraction of the  $p$ -polarized normally-incident light, which in turn determines the resonant frequency  $\omega_{\text{sp}}$  of the surface plasmon-polariton mode.

In order for us to explicitly determine the electric field dependence for  $\mathcal{P}^{\text{loc}}(\mathbf{r}; \omega)$ , we now turn to the quantum kinetics of electrons in a quantum dot. Here, the optical polarization field  $\mathcal{P}^{\text{loc}}(\mathbf{r}; \omega)$  plays a unique role in bridging the gap between the classical Maxwell's equations for electromagnetic fields and the quantum-mechanical Schrödinger equation for electrons. The quantum kinetics of electrons in photo-excited quantum dots should be adequately described by the so-called semiconductor Bloch equations [6–8] which are a generalization of the well-known optical Bloch equations in two ways, namely the incorporation of electron scattering by impurities, phonons and other electrons, as well as the many-body effects on dephasing in the photo-induced optical coherence.

For photo-excited spin-degenerate electrons (holes) in the conduction (valence) band, their semiconductor Bloch equations with  $\ell(j) = 1, 2, \dots$  are given, within the rotating-wave approximation, by

$$\frac{dn_{\ell(j)}^{\text{e(h)}}}{dt} = \frac{2}{\hbar} \sum_{j(\ell)} \text{Im} \left[ (Y_\ell^j)^* (\mathcal{M}_{\ell,j}^{\text{eh}} - Y_\ell^j V_{\ell,j;j,\ell}^{\text{eh}}) \right] + \left. \frac{\partial n_{\ell(j)}^{\text{e(h)}}}{\partial t} \right|_{\text{rel}} - \delta_{\ell(j),1} \mathcal{R}_{\text{sp}} n_1^{\text{e}} n_1^{\text{h}}, \quad (5)$$

where  $\mathcal{R}_{\text{sp}}$  is the spontaneous emission rate, which should be calculated by using the Kubo-Martin-Schwinger relation [16] and including band gap energy and interband dipole moment renormalizations, and  $n_{\ell(j)}^{\text{e(h)}}$  represents the electron (hole) level population. In Eq. (5), the Boltzmann-type scattering term for non-radiative energy relaxation of electrons (holes) is  $\left. \frac{\partial n_{\ell(j)}^{\text{e(h)}}}{\partial t} \right|_{\text{rel}} = \mathcal{W}_{\ell(j)}^{\text{in}} (1 - n_{\ell(j)}^{\text{e(h)}}) - \mathcal{W}_{\ell(j)}^{\text{out}} n_{\ell(j)}^{\text{e(h)}}$ , where  $\mathcal{W}_{\ell(j)}^{\text{in}}$  and  $\mathcal{W}_{\ell(j)}^{\text{out}}$  are the scattering-in and scattering-out rates for electrons (holes), respectively, and should be calculated by including carrier-carrier and carrier-(optical) phonon interactions. Moreover, we know from Eq. (5) that the total number  $N_{\text{e(h)}}(t)$  of photo-excited electrons (holes) is conserved.

The induced optical polarization in the semiconductor Bloch equations with  $\ell(j) = 1, 2, \dots$  satisfies the following equations for a spin-averaged e-h plasma, i.e.,

$$i\hbar \frac{d}{dt} Y_\ell^j = \left[ \bar{\varepsilon}_\ell^{\text{e}}(\omega|t) + \bar{\varepsilon}_j^{\text{h}}(\omega|t) - \hbar(\omega + i\gamma_0) \right] Y_\ell^j + (1 - n_\ell^{\text{e}} - n_j^{\text{h}}) (\mathcal{M}_{\ell,j}^{\text{eh}} - Y_\ell^j V_{\ell,j;j,\ell}^{\text{eh}})$$

$$\begin{aligned}
& + Y_\ell^j \left[ \sum_{j_1} n_{j_1}^h \left( V_{j,j_1;j_1,j}^{\text{hh}} - V_{j,j_1;j,j_1}^{\text{hh}} \right) - \sum_{\ell_1} n_{\ell_1}^e V_{\ell_1,j;j,\ell_1}^{\text{eh}} \right] \\
& + Y_\ell^j \left[ \sum_{\ell_1} n_{\ell_1}^e \left( V_{\ell,\ell_1;\ell_1,\ell}^{\text{ee}} - V_{\ell,\ell_1;\ell,\ell_1}^{\text{ee}} \right) - \sum_{j_1} n_{j_1}^h V_{\ell,j_1;j_1,\ell}^{\text{eh}} \right] , \tag{6}
\end{aligned}$$

where  $Y_\ell^j$  represents the induced interband optical coherence,  $\hbar\gamma_0 = \hbar\gamma_{\text{eh}} + \hbar\gamma_{\text{ext}}$  is the energy level broadening (due to finite carrier lifetime plus the radiation loss of an external evanescent field),  $\bar{\varepsilon}_{\ell(j)}^{\text{e(h)}}(\omega|t)$  is the kinetic energy of dressed single electrons (holes) (see supplementary materials). In Eq. (6), the diagonal dephasing of  $Y_\ell^j$ , the renormalization of interband Rabi coupling, the renormalization of electron and hole energies, as well as the exciton binding energy, are all taken into account. Since the e-h plasma is not spin-dependent, they may be excited by both left and right circularly polarized light. The off-diagonal dephasing of  $Y_\ell^j$  has been neglected due to low carrier density in quantum dots. In Eqs.(5) and (6), we have introduced the Coulomb matrix elements  $V_{\ell_1,\ell_2;\ell_3,\ell_4}^{\text{ee}}$ ,  $V_{j_1,j_2;j_3,j_4}^{\text{hh}}$  and  $V_{\ell,j;j',\ell'}^{\text{eh}}$ , for electron-electron, hole-hole and e-h interactions, respectively.

The steady-state solution of Eq. (6), i.e., subject to the condition that  $dY_\ell^j/dt = 0$ , has been obtained as

$$Y_\ell^j(t|\omega) = \left[ \frac{1 - n_\ell^e(t) - n_j^h(t)}{\hbar(\omega + i\gamma_0) - \hbar\bar{\Omega}_{\ell,j}^{\text{eh}}(\omega|t)} \right] \mathcal{M}_{\ell,j}^{\text{eh}}(t) , \tag{7}$$

where the photon and Coulomb renormalized interband energy level separation  $\hbar\bar{\Omega}_{\ell,j}^{\text{eh}}(\omega|t)$  is given by

$$\begin{aligned}
\hbar\bar{\Omega}_{\ell,j}^{\text{eh}}(\omega|t) &= \bar{\varepsilon}_\ell^e(\omega|t) + \bar{\varepsilon}_j^h(\omega|t) - V_{\ell,j;j,\ell}^{\text{eh}} + \sum_{\ell_1} n_{\ell_1}^e(t) \left( V_{\ell,\ell_1;\ell_1,\ell}^{\text{ee}} - V_{\ell,\ell_1;\ell,\ell_1}^{\text{ee}} \right) \\
&+ \sum_{j_1} n_{j_1}^h(t) \left( V_{j,j_1;j_1,j}^{\text{hh}} - V_{j,j_1;j,j_1}^{\text{hh}} \right) - \sum_{\ell_1 \neq \ell} n_{\ell_1}^e(t) V_{\ell_1,j;j,\ell_1}^{\text{eh}} - \sum_{j_1 \neq j} n_{j_1}^h(t) V_{\ell,j_1;j_1,\ell}^{\text{eh}} , \tag{8}
\end{aligned}$$

and the matrix elements employed in Eqs. (5) and (6) for the Rabi coupling between photoexcited carriers and an evanescent pump field  $\mathbf{E}(\mathbf{r}; t) = \theta(t) \mathbf{E}(\mathbf{r}; \omega) e^{-i\omega t}$  are given by

$$\mathcal{M}_{\ell,j}^{\text{eh}}(t) = -\delta_{\ell,1} \delta_{j,1} \theta(t) \left[ \mathbf{E}_{\ell,j}^{\text{eh}}(\omega) \cdot \mathbf{d}_{\text{c,v}} \right] . \tag{9}$$

In this notation,  $\theta(x)$  is the Heaviside unit step function, the static interband dipole moment denoted by  $\mathbf{d}_{\text{c,v}}$  is given by [17, 18] (see supplementary materials)

$$\mathbf{d}_{c,v} = \int d^3\mathbf{r} [u_c(\mathbf{r})]^* \mathbf{r} u_v(\mathbf{r}) = \mathbf{d}_{c,v}^* , \quad (10)$$

where  $u_c(\mathbf{r})$  and  $u_v(\mathbf{r})$  are the Bloch functions associated with conduction and valence bands at the  $\Gamma$ -point in the first Brillouin zone of the host semiconductor, and the effective electric field coupled to the quantum dot is evaluated by

$$\mathbf{E}_{\ell,j}^{\text{eh}}(\omega) = \int d^3\mathbf{r} [\psi_\ell^e(\mathbf{r})]^* \mathbf{E}(\mathbf{r}; \omega) [\psi_j^h(\mathbf{r})]^* , \quad (11)$$

where  $\psi_{\ell(j)}^{e(h)}(\mathbf{r})$  is the envelope function of electrons (holes) in the quantum dot. Next, the photo-induced interband optical polarization  $\mathcal{P}^{\text{loc}}(\mathbf{r}; \omega)$  by dressed electrons in the quantum dot is given by [2]

$$\begin{aligned} \mathcal{P}^{\text{loc}}(\mathbf{r}; \omega) &= 2 |\xi_{\text{QD}}(\mathbf{r})|^2 \mathbf{d}_{c,v} \left\{ \int d^3\mathbf{r}' \psi_1^e(\mathbf{r}') \psi_1^h(\mathbf{r}') \right\} \\ &\times \frac{1}{\hbar} \lim_{t \rightarrow \infty} \left[ \frac{1 - n_1^e(t) - n_1^h(t)}{\omega + i\gamma_0 - \overline{\Omega}_{1,1}^{\text{eh}}(\omega|t)} \right] \mathcal{M}_{1,1}^{\text{eh}}(t) , \end{aligned} \quad (12)$$

where the profile function  $|\xi_{\text{QD}}(\mathbf{r})|^2$  comes from the quantum confinement inside a quantum dot.

In our numerical calculations, we chose the quantum dot dimensions as 210 Å and 100 Å for along the  $x$  and  $y$  directions, respectively,  $m_e^* = 0.067 m_0$  and  $m_h^* = 0.62 m_0$  for the electron and hole effective masses, in terms of the free electron mass  $m_0$ ,  $\theta_0 = 45^\circ$ ,  $x_{1g} = x_{2g} = 610$  Å,  $\epsilon_b = 12$  for the quantum dot,  $\epsilon_d = 12$  for the cladding layer,  $\epsilon_s = 11$  and  $\epsilon_\infty = 13$  for the static and optical dielectric constants,  $\hbar\Omega_0 = 36$  meV for the energy of optical phonons,  $\hbar\Gamma_{\text{ph}} = 3$  meV ( $= \hbar\gamma_0$ ) for the phonon broadening,  $z_0 = 610$  Å, and  $T = 300$  K for the lattice temperature. The silver plasma frequency is  $13.8 \times 10^{15}$  Hz and the silver plasma dephasing parameter is  $0.1075 \times 10^{15}$  Hz. The energy gap  $E_G$  for the active quantum-dot material is 1.927 eV at  $T = 300$  K.

Figure 1 presents the absorption coefficient  $\beta_0(\omega_{\text{sp}})$  for an SPP wave by a quantum dot [16], the scattering field  $|\mathbf{E}_{\text{tot}} - \mathbf{E}_{\text{sp}}|$  of the SPP wave, and the energy-level occupations for electrons  $n_{\ell,e}$  and holes  $n_{j,h}$  with  $\ell, j = 1, 2$  as functions of the frequency detuning  $\Delta\hbar\omega_{\text{sp}} \equiv \hbar\omega_{\text{sp}} - (E_G + \varepsilon_{1,e} + \varepsilon_{1,h})$  with bare energies  $\varepsilon_{1,e}, \varepsilon_{1,h}$  for ground-state electrons and holes. A dip is observed at resonance  $\Delta\hbar\omega_{\text{sp}} = 0$  in the upper-left panel, which becomes deeper with decreasing amplitude  $E_{\text{sp}}$  of the SPP wave in the strong-coupling regime due

to a reduction of saturated absorption. However, this dip disappears when  $E_{\text{sp}}$  drops to 25 kV/cm in the weak-coupling limit due to the suppression of the photon dressing effect, which is accompanied by a one-order of magnitude increase in the absorption-peak strength. The dip in the upper-left panel corresponds to a peak in the scattering field, as may be seen from the upper-right panel of this figure. The scattering field increases with the frequency detuning away from resonance, corresponding to decreasing absorption. Consequently, two local minima appear on both sides of resonance for the scattering field in the strong-coupling regime. Maxwell-Bloch equations couple the field dynamics outside a quantum dot with the electron dynamics inside the dot. At  $E_{\text{sp}} = 125$  kV/cm in the lower-right-hand panel, we obtain peaks in energy-level occupations at resonance, which are broadened by the finite carrier lifetime as well as the optical power of the SPP wave. Moreover, jumps in the energy level occupation may be seen at resonance due to Rabi splitting of the energy levels in the dressed electron states. The effect of resonant phonon absorption also plays a significant role in the finite value of  $n_{2,e}$  with energy-level separations  $\varepsilon_{2,e} - \varepsilon_{1,e} \approx \hbar\Omega_0$ . However, as  $E_{\text{sp}}$  decreases to 25 kV/cm in the lower-left panel, peaks in the energy-level occupations are greatly sharpened and negatively shifted due to the suppression of the broadening from the optical power and the excitonic effect, respectively. Additionally, jumps in the energy level occupations become invisible because the Rabi-split energy gap in this case is much smaller than the energy-level broadening from the finite lifetime of electrons (i.e., substantially dampened Rabi oscillations between the first electron and hole levels).

Although the interband dipole moment of a quantum dot is isotropic in space, the scattering field (see Fig. 2 with  $E_{\text{sp}} = 150$  kV/cm) in the  $x$  direction (upper panel) and in the  $z$  direction (lower panel) are still different due to the presence of a metallic surface perpendicular to the  $z$  direction in our system. However, this isotropic intensity distribution is mostly recovered at  $\Delta\hbar\omega_{\text{sp}} = 0$ . Specifically, the scattering field in the  $z$  direction is one order of magnitude larger than that in the  $x$  direction. The field pattern in the lower panel tends to spread in the  $z$  direction, while the pattern in the upper panel distributes in the  $x$  direction. From this figure, we also find that the intensities in both panels follow the pattern of strong-weak-strong-weak-strong as the frequency detuning is swept across  $\Delta\hbar\omega_{\text{sp}} = 0$ , which agrees with the observation of the scattering field at the quantum dot in the upper-right panel of Fig. 1.



Color maps for the scattering field around a quantum dot displayed in Fig. 2 are for strong coupling between the dot and an SPP wave. We present in Fig. 3 the scattering field maps in the weak-coupling regime, where the strong-weak-strong-weak-strong pattern in the strong-coupling regimes has been changed to a weak-strong-weak pattern. Moreover, the SPP-wave frequency for the resonant scattering field has been shifted from  $\Delta\hbar\omega_{\text{sp}} = 0$  to  $\Delta\hbar\omega_{\text{sp}} = 1$  meV, demonstrating a positive depolarization shift of the optical excitation energy, as may be verified from the upper left-hand panel of Fig. 1. However, this depolarization effect is completely masked by the occurrence of a local minimum at  $E_{\text{sp}} = 150$  kV/cm.

In conclusion, for a strong SPP wave, we have demonstrated the unique effect of its resonant scattering by a dynamical semiconductor quantum dot very close to the metal/dielectric interface. We have also predicted correlation between a resonant peak in the scattering field spectrum and a resonant local minimum in the absorption spectrum of the SPP wave.

In this Letter, we only investigated the coupling between an SPP wave and a single quantum dot for the simplest case. Our formalism may be generalized in a straightforward way to include multiple quantum dots close to the surface of a metallic film. The open surface of the metallic film provides an easy solution to perform biochemical and biomedical tests under a microscope in a laboratory setting. If the quantum dots are further coated with specially-selected chemically-reactive molecules, they should be expected to be able to adhere to special target tissue if the chemical properties are matched with each other. Therefore, the spontaneous emission by electrons in these quantum dots may be employed non-invasively for near-field imaging of target tissue with very high brightness and spatial resolution.

Additionally, instead of coupling to the lowest pair of e-h energy levels, we may choose the surface plasmon frequency for a resonant coupling to the next pair of e-h levels. In this case, optical pumping from the localized surface plasmon field may transfer a population inversion from the excited pair to the ground pair of e-h levels by exchanging thermal energy with lattice phonons, leading to a possible lasing action. Such a surface plasmon based quantum-dot laser would have a beam size as small as a few nanometers (not limited by its wavelength), which is expected to be very useful to spatially selective illumination of individual molecules (neuron cells) in low-temperature photo-excited chemical reactions (optogenetics and neuroscience).

## Acknowledgments

DH would like to acknowledge the support by the Air Force Office of Scientific Research (AFOSR). This research was also supported by contract # FA 9453-13-1-0291 of AFRL.

---

- [1] G. Gumbs and D. H. Huang, *Properties of Interacting Low-Dimensional Systems* (Wiley-VCH Verlag GmbH & Co. kGaA, Weinheim, Germany, 2011), Chaps. 4 and 5.
- [2] S. Schmitt-Rink, D. S. Chemla and H. Haug, “Nonequilibrium theory of the optical Stark effect and spectral hole burning in semiconductors”, *Physical Review B* **37**, 941 (1988).
- [3] D. Dini, R. Köhler, A. Tredicucci, G. Biasiol and L. Sorba, “Microcavity polariton splitting of intersubband transitions”, *Physical Review Letters* **90**, 116401 (2003).
- [4] Y. Todorov, A. M. Andrews, I. Sagnes, R. Colombelli, P. Klang, G. Strasser and C. Sirtori, “Strong-light-matter coupling in subwavelength metal-dielectric microcavities at terahertz frequencies”, *Physical Review Letters* **102**, 186402 (2009).
- [5] Y. Todorov, A. M. Andrews, R. Colombelli, S. De Liberato, C. Ciuti, P. Klang, G. Strasser and C. Sirtori, “Ultrastrong light-matter coupling regime with polariton dots”, *Physical Review Letters* **105**, 196402 (2010).
- [6] F. Rossi and T. Kuhn, “Theory of ultrafast phenomena in photoexcited semiconductors”, *Review of Modern Physics* **74**, 895 (2002).
- [7] V. M. Axt and T. Kuhn, “Femtosecond spectroscopy in semiconductors: a key to coherences, correlations and quantum kinetics”, *Reports on Progress in Physics* **67**, 433 (2004).
- [8] M. Kira and S. W. Koch, “Many-body correlations and excitonic effects in semiconductor spectroscopy”, *Progress in Quantum Electronics* **30**, 155 (2006).
- [9] F. Jahnke, M. Kira and S. W. Koch, “Linear and nonlinear optical properties of excitons in semiconductor quantum wells and microcavities”, *Zeitschrift für Physik B* **104**, 559 (1997).
- [10] J. A. Sánchez-Gil and A. A. Maradudin, “Dynamic near-field calculations of surface-plasmon polariton pulses resonantly scattered at sub-micron metal defects”, *Optics Express* **12**, 883 (2004).
- [11] R. E. Arias and A. A. Maradudin, “Scattering of a surface plasmon polariton by a localized dielectric surface defect”, *Optics Express* **21**, 9734 (2013).

- [12] F. Pincemin, A. Sentenac and J.-J. Greffet, “*Near-field scattered by a dielectric rod below a metallic surface*”, Journal of Optical Society of American A **11**, 1117 (1994).
- [13] A. A. Maradudin and D. L. Mills, “*The attenuation of Rayleigh surface waves by surface roughness*”, Annals of Physics **100**, 262 (1976).
- [14] A. A. Maradudin and D. L. Mills, “*Scattering and absorption of electromagnetic radiation by a semi-infinite medium in the presence of surface roughness*”, Physical Review B **11**, 1392 (1975).
- [15] M. G. Cottam and A. A. Maradudin, “Surface linear response functions”, in *Surface Excitations*, Eds. V. M. Agranovich and R. Loudon (North-Holland, Amsterdam, 1984), pp. 1-194.
- [16] D. H. Huang and P. M. Alsing, “*Many-body effects on optical carrier cooling in intrinsic semiconductors at low lattice temperatures*”, Physical Review B **78**, 035206 (2008).
- [17] E. O. Kane, “*Band structure of indium antimonide*”, Journal of Physics and Chemistry of Solids **1**, 249 (1957).
- [18] U. Bockelmann and G. Bastard, “*Interband absorption in quantum wires. I. Zero-magnetic-field case*”, Physical Review B **45**, 1688 (1992).

## Appendix A: ELECTRONIC STATES OF A QUANTUM DOT

We have employed a box-type potential with hard walls for a quantum dot, which is given by

$$V(\mathbf{r}) = \begin{cases} 0, & 0 \leq x_i \leq L_i \text{ for } i = 1, 2, 3 \\ \infty, & \text{others} \end{cases}, \quad (\text{A1})$$

where the position vector  $\mathbf{r} = (x_1, x_2, x_3)$ ,  $L_1$ ,  $L_2$  and  $L_3$  are the widths of the potential in the  $x_1$ ,  $x_2$  and  $x_3$  directions, respectively. The Schrödinger equation for a single electron or hole in a quantum dot is written as

$$-\frac{\hbar^2}{2m^*} \left[ \frac{\partial^2}{\partial x_1^2} + \frac{\partial^2}{\partial x_2^2} + \frac{\partial^2}{\partial x_3^2} + V(\mathbf{r}) \right] \psi(\mathbf{r}) = \varepsilon \psi(\mathbf{r}), \quad (\text{A2})$$

where the effective mass  $m^*$  is  $m_e^*$  for electrons or  $m_h^*$  for holes. The eigenstate wave function associated with Eq. (A2) is found to be

$$\psi_{n_1, n_2, n_3}(\mathbf{r}) = \sqrt{\frac{2}{L_1}} \sin \left[ \left( \frac{n_1 \pi}{L_1} \right) x_1 \right] \sqrt{\frac{2}{L_2}} \sin \left[ \left( \frac{n_2 \pi}{L_2} \right) x_2 \right] \sqrt{\frac{2}{L_3}} \sin \left[ \left( \frac{n_3 \pi}{L_3} \right) x_3 \right], \quad (\text{A3})$$

which is same for both electrons and holes, and the eigenstate energy associated with Eq.(A2) is

$$\varepsilon_{n_1, n_2, n_3} = \frac{\hbar^2}{2m^*} \left[ \left( \frac{n_1 \pi}{L_1} \right)^2 + \left( \frac{n_2 \pi}{L_2} \right)^2 + \left( \frac{n_3 \pi}{L_3} \right)^2 \right], \quad (\text{A4})$$

where the quantum numbers  $n_1, n_2, n_3 = 1, 2, \dots$ .

By using the calculated bare energy levels in Eq. (A4), the dressed electron ( $\lambda_\alpha^e$ ) and hole ( $\lambda_\alpha^h$ ) energy levels under the rotating wave approximation take the form of

$$\lambda_\alpha^e(\omega|t) = \lambda_\alpha^h(\omega|t) = \begin{cases} \frac{1}{2} \left( \hbar\omega + \sqrt{[\mathcal{E}_G(T) + \varepsilon_\alpha^e + \varepsilon_\alpha^h - \hbar\omega]^2 + 4|\mathcal{M}_{\alpha,\alpha}^{\text{eh}}(t)|^2} \right) \\ \quad \text{if } \hbar\omega \leq \mathcal{E}_G(T) + \varepsilon_\alpha^e + \varepsilon_\alpha^h \\ \\ \frac{1}{2} \left( \hbar\omega - \sqrt{[\mathcal{E}_G(T) + \varepsilon_\alpha^e + \varepsilon_\alpha^h - \hbar\omega]^2 + 4|\mathcal{M}_{\alpha,\alpha}^{\text{eh}}(t)|^2} \right) \\ \quad \text{if } \hbar\omega \geq \mathcal{E}_G(T) + \varepsilon_\alpha^e + \varepsilon_\alpha^h \end{cases}, \quad (\text{A5})$$

where the composite index  $\alpha = \{n_1, n_2, n_3\}$ . Moreover, we get the energy levels of dressed electrons in the lab frame, i.e.,  $\bar{\varepsilon}_\alpha^e(\omega|t) = \lambda_\alpha^e(\omega|t) + (\varepsilon_\alpha^e - \varepsilon_\alpha^h)/2$  and  $\bar{\varepsilon}_\ell^e(\omega|t) = \varepsilon_\ell^e + \mathcal{E}_G(T)/2$  for  $\ell \neq \alpha$ . Similarly, we obtain the energy levels of dressed holes  $\bar{\varepsilon}_\alpha^h(\omega|t) = \lambda_\alpha^h(\omega|t) + (\varepsilon_\alpha^h - \varepsilon_\alpha^e)/2$  and  $\bar{\varepsilon}_j^e(\omega|t) = \varepsilon_j^h + \mathcal{E}_G(T)/2$  for  $j \neq \alpha$ .

The interband dipole moment  $\mathbf{d}_{c,v} = d_{c,v} \hat{\mathbf{e}}_d$  at the isotropic  $\Gamma$ -point can be calculated according to the Kane approximation

$$d_{c,v} = \sqrt{\frac{e^2 \hbar^2}{2m_0 \mathcal{E}_G(T)} \left( \frac{m_0}{m_e^*} - 1 \right)}. \quad (\text{A6})$$

Furthermore, the direction of the dipole moment  $\hat{\mathbf{e}}_d$  is determined by the quantum-dot energy levels in resonance with the photon energy  $\hbar\omega$ .

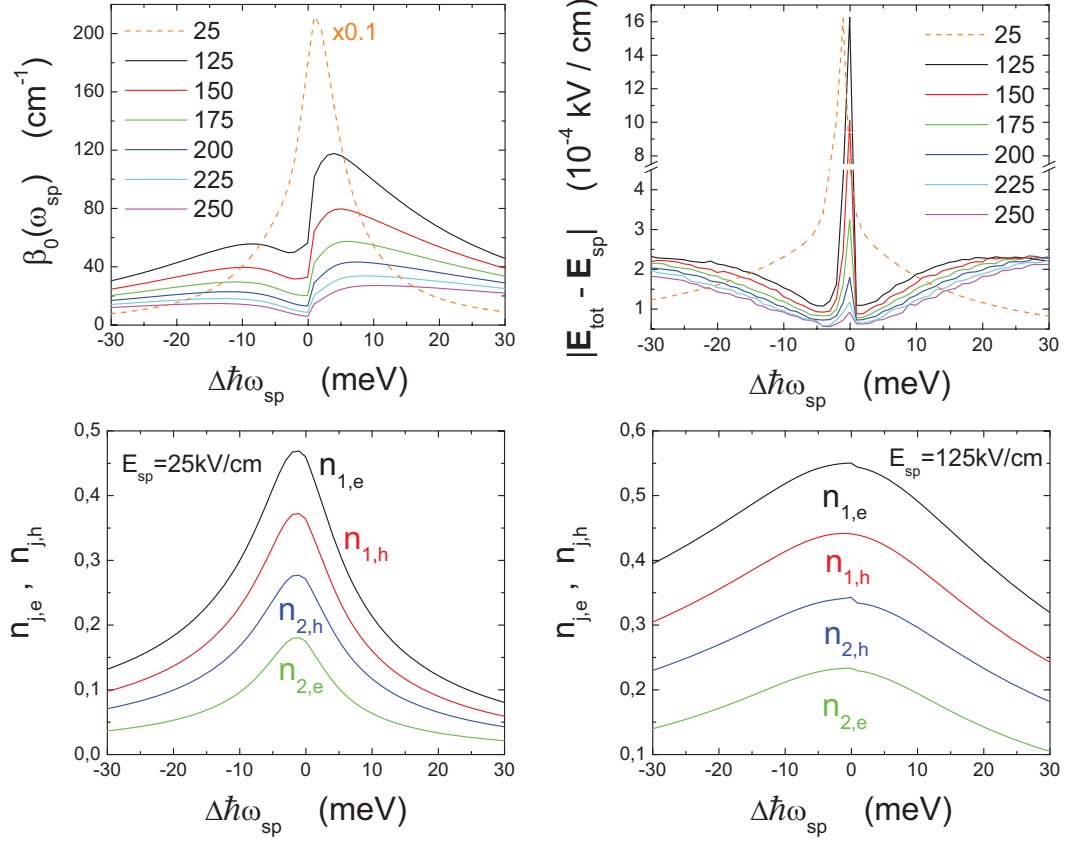


FIG. 1: (Color online) Absorption coefficients  $\beta_0(\omega_{\text{sp}})$  (upper-left) and scattering field  $|\mathbf{E}_{\text{tot}} - \mathbf{E}_{\text{sp}}|$  at the quantum dot (upper-right), as well as the energy-level occupations for electrons  $n_{\ell,e}$  and holes  $n_{j,h}$  (lower) as functions of the frequency detuning  $\Delta\hbar\omega_{\text{sp}}$  (see text). The results for various amplitudes  $E_{\text{sp}}$  of an SPP wave with frequency  $\omega_{\text{sp}}$  are presented in the upper panels, along with a comparison of the energy-level occupations for  $E_{\text{sp}} = 25$  and  $125$  kV/cm in the lower panels. The label  $\times 0.1$  in the upper panel indicates that the result is multiplied by a factor of 0.1.

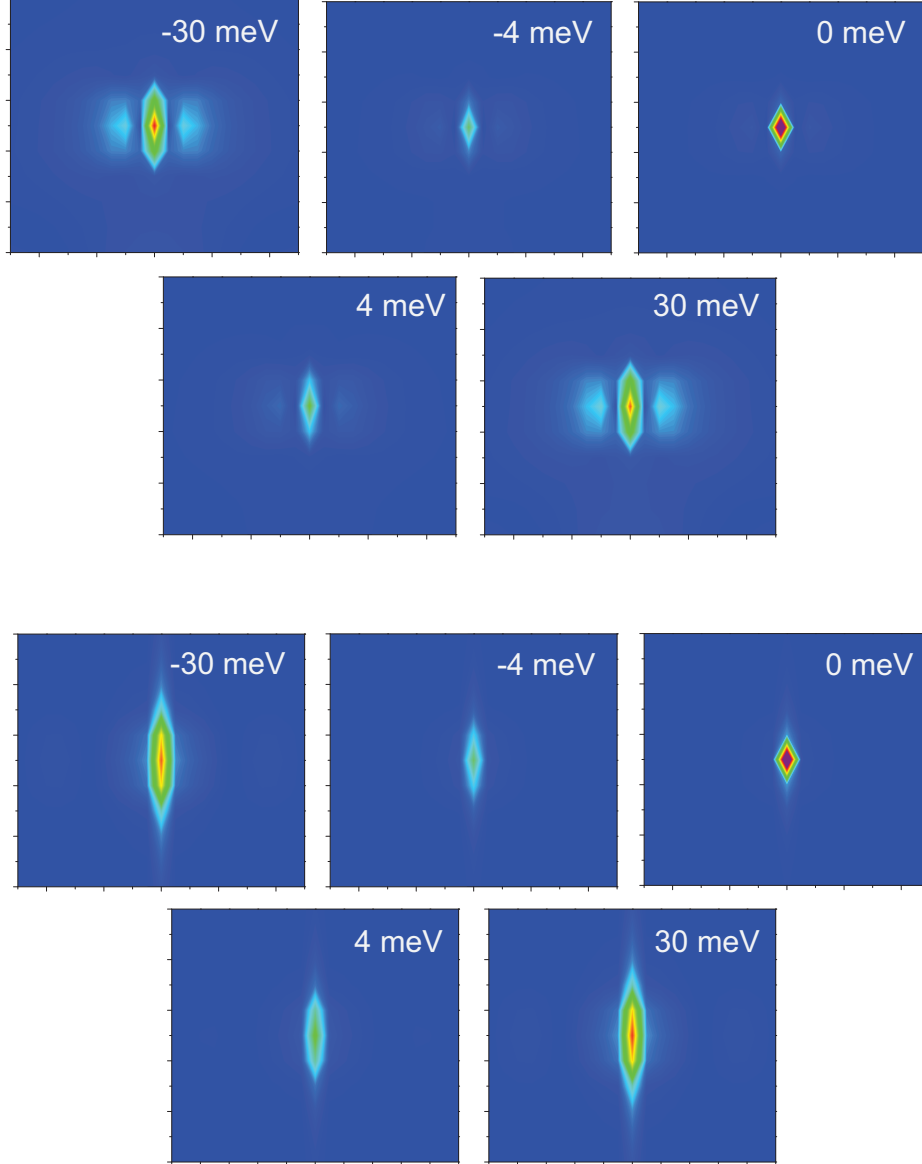


FIG. 2: (Color online) Scattering field color maps for  $|E_{\text{tot}}^\nu - E_{\text{sp}}^\nu|/E_{\text{sp}}$  (with  $y = 0$ ) around a quantum dot above a metallic surface in the  $x$  ( $\nu = 1$ , upper panel) and  $z$  ( $\nu = 3$ , lower panel) directions, respectively, with varying frequency detuning  $\Delta\hbar\omega_{\text{sp}} = -30, -4, 0, 4$  and  $30$  meV. We chose  $E_{\text{sp}} = 150$  kV/cm. The color scales (blue-to-red) for all values of  $\Delta\hbar\omega_{\text{sp}}$  are  $0-1 \times 10^{-7}$  in the upper panel and  $0-1.6 \times 10^{-6}$  in the lower panel except for  $\Delta\hbar\omega_{\text{sp}} = 0$  where the color scales are  $0-4.5 \times 10^{-7}$  in the upper panel and  $0-7 \times 10^{-6}$  in the lower panel. The use of different scales is to clearly display spatial changes in the intensity distribution.

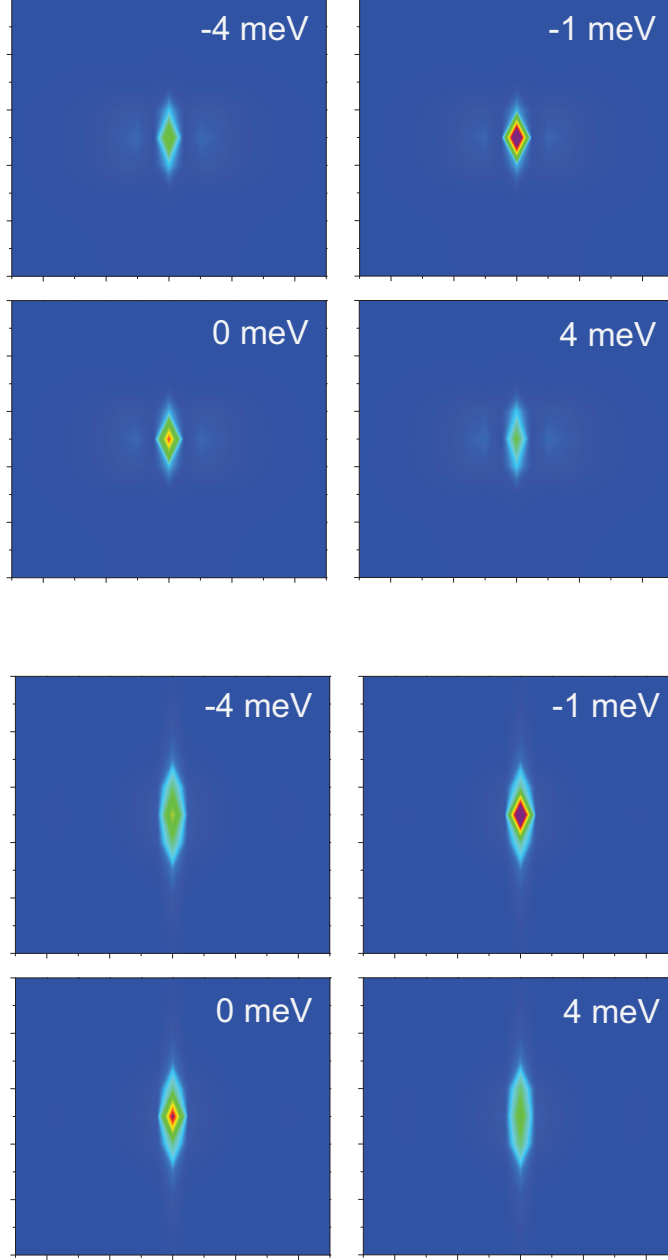


FIG. 3: (Color online) Scattering field color maps for  $|E_{\text{tot}}^\nu - E_{\text{sp}}^\nu|/E_{\text{sp}}$  (with  $y = 0$ ) around a quantum dot above the metallic surface in the  $x$  ( $\nu = 1$ , upper panel) and  $z$  ( $\nu = 3$ , lower panel) directions, respectively, with varying frequency detuning  $\Delta\hbar\omega_{\text{sp}} = -4, -1, 0$  and  $4$  meV. Here,  $E_{\text{sp}} = 25$  kV/cm is assumed. The color scales (blue-to-red) for all values of  $\Delta\hbar\omega_{\text{sp}}$  are  $0-1.4 \times 10^{-6}$  in the upper panel and  $0-2 \times 10^{-5}$  in the lower panel except for  $\Delta\hbar\omega_{\text{sp}} = -1$  meV where the color scales are  $0-4 \times 10^{-6}$  in the upper panel and  $0-7 \times 10^{-5}$  in the lower panel. Again, the use of different scales is for a clear display of spatial changes in the intensity distribution.